Engineering and Technology Journal
Journal homepage: https://etj.uotechnology.edu.iq

Studying the influence of variable inlet guide vane with the physical faults on the performance of industrial gas turbine at part-load operation

Waleligne M. Salilew[a]*, Zainal A. Abdul Karim[b], Tamiru A. Lemma[a]

[a] Mechanical Engineering Dept., Universiti Teknologi PETRONAS, Bandar Seri Iskandar 32610, Perak, Malaysia.
[b] Centre for Automotive Research and Electric Mobility (CAREM), Universiti Teknologi PETRONAS, 32610 Seri Iskandar, Perak, Malaysia.
*Corresponding author Email: waleligne_20001048@utp.edu.my

HIGHLIGHTS

- Effects of drift, fouling, and erosion on gas turbine efficiency and output are investigated.
- Fouling impacts upstream, while erosion affects downstream components in gas turbines.
- Research findings support ML-based fault detection for optimal turbine maintenance.

ARTICLE INFO

Handling editor: Sattar Aljabair

Keywords:

Variable inlet guide vane

Gas turbine performance

Fouling

Erosion

Performance degradation

ABSTRACT

This research work presents a gas turbine performance investigation. Researchers have put efforts into this field of study; however, the influence of the concurrence of variable inlet guide vane (VIGV) drift, fouling, and erosion on the three-shaft gas turbine's performance during part-load operation has remained unexplored. Therefore, this study addresses this gap. First the gas turbine design point and off-design performance model have been developed by utilizing the original engine manufacturer data provided. The accuracy of the models was validated, and the maximum mean absolute percentage error of the design point performance model is shown at exhaust temperature prediction, it is about 1.74%. The off-design performance model was also validated with the power output versus ambient temperature and efficiency versus operating curves. At each operational point, the power output versus ambient temperature error from the validation data was 0.02%, while the efficiency versus ambient temperature error was 4.5%. After the validation, the engine model was subjected to the concurrence of variable inlet guide vane drift, fouling, and erosion conditions to simulate the degradation state. The results show that the highest isentropic efficiency deviation due to component faults occurred in the upstream components, specifically in the low-pressure compressor's (LPC) isentropic efficiency. The deviation recorded due to the concurrence of VIGV drift at -6.5° and 100% fouling severity is -11.47%, whereas 9.65% is the LPC isentropic efficiency deviation recorded when VIGV drift at -6.5° and erosion at 100% severity level simultaneously occurred. In addition, the effects of the faults above on gas path measurements were simulated, and the highest measurement deviation was observed when simultaneous LPC fouling and -6.5% VIGV drift occurred. Among the measurements, the highest deviation was observed in the exhaust temperature and thermal efficiency, about 9.23% and -7.35%, respectively.

1. Introduction

A gas turbine operates on the principle of converting the energy of a flowing gas into mechanical power. It consists of three primary components: the compressor, the combustion chamber, and the turbine [1]. The process begins with the compressor, which draws in ambient air and compresses it, thereby increasing its pressure. The compressed air enters the combustion chamber, where fuel is injected and ignited. The resulting combustion releases a high-temperature, high-pressure gas stream. This hot gas expands and flows through the turbine, comprising a series of blades or vanes. As the gas passes over the turbine blades, the energy transfer will occur, causing the turbine to rotate [2,3]. The rotation of the turbine is used to drive the compressor and any attached machinery, such as a generator. After exiting the turbine, the lower-pressure gas is typically directed to a waste heat recovery system, which can be utilized for various purposes, such as heating or powering additional equipment. The continuous airflow through the gas turbine allows for sustained operation, and the process repeats itself to maintain constant power output. The efficiency of a gas turbine is determined by factors such as the compression ratio, combustion efficiency, and

http://doi.org/10.30684/etj.2023.139204.1471
Received 31 May 2023; Received in revised form 11 July 2023; Accepted 25 July 2023; Available online 25 August 2023
2412-0758/University of Technology-Iraq, Baghdad, Iraq

turbine design, all of which can be optimized to improve overall performance. Modern gas turbines are designed with advanced aerodynamics and materials to maximize efficiency and power output. They are widely used in oil and gas, power generation, aviation, and industrial applications, providing a reliable and efficient means of converting gas energy into useful work [4,5].
A gas turbine is a thermal machine with mechanical, electrical, and hydraulic systems that works under severe stress, high pressure, high temperature, and high speed [1]. The tip clearance variations in the rotating components, actuator wear, seal wear, blade erosion, blade fouling, blade warping, blocked fuel nozzles, sensor issues, and domestic object damage and foreign object damage are the factors that contribute to a decline in the gas turbine performance over time[4-6]. Due to harsh operating conditions, the performance of the gas turbine steadily declines over time. Anomalous working conditions must be avoided as soon as possible to reduce the associated increase in energy consumption and environmental damage. Even though the engine usually works because of having a decent inlet filtration system to use clean air, the parts of the engine flow stream will become eroded, corroded, covered in rust scale, and damaged [7]. To evaluate the gas turbine's overall performance and satisfy operational and maintenance requirements, knowledge of the gas turbine's fundamental state is crucial [8]. Several commercial simulation software has helped create certain engine performance models [9]. The software helps to develop both steady-state and transient performance models, and the developed performance model will be used to simulate the gas turbine at both clean and deteriorated conditions [10].

Modern gas turbines include advanced features for improved reliability, availability, and sustainability [11]. Variable geometry in compressors and turbines, which comprises variable inlet guide vane (VIGV), variable stator vanes (VSVs), variable bleed valve (VBV), and variable area nozzle (VAN) are some of the features that increase the performance of the gas turbine [12]. The variable inlet guide vane is scheduled as a function of spool speed, and this helps the gas turbine maintain its performance when the engine experiences a speed fluctuation during startup, shutdown, and load changes [13]. Surging and stalling frequently occurring at low speeds during startup and shutdowns decline the engine's performance [14]. Therefore, the VIGVs and bleed control system can improve engine performance by removing compressor surge phenomena. Different connections attached to guiding vanes are part of an actuation system to regulate the VIGVs [15]. The VIVGs could have various issues, like drifting beyond the standard functioning range. These issues and faults will finally cause an unexpected shutdown due to surges and choking in the compressor stages. Other problems, such as variable geometry mechanism faults, axial compressor fouling, and increasing ambient temperature, may also contribute to degradation [16]. Salar et al. [17], identified that low-speed stop, high-speed stop, hydraulic ram leakage, and Rotary variable displacement transducer (RVDT) misalignment are the main causes of VIGV drift. According to Tsalavoutas et al. [18], other factors, such as the wearing of the actuation mechanism linkages and the misalignment or stacking of the vanes because of loosened bolts, caused VIGVs to deviate from their typical schedule. Continuous monitoring is required to ensure that the movement and position of the actuation mechanism are in sync with the actual design schedule to avoid these issues. The difficulty of monitoring the position of an actuation mechanism for many vanes makes this solution impractical. To overcome this, an adaptive performance model to identify VIGV problems was proposed by Stamatis et al. [19]. By artificially introducing various VIGV drifts, some researchers have attempted to observe the impact of VIGV drift on gas turbine performance. To investigate the impact of VIGV drift on the compressor's performance, Cruz-Manzo et al. [20], recently created a MATLAB Simulink-based performance model. A comparison of the difference between the position that the VIGV was intended to be in and the drift position was investigated, and a significant variation has been observed. Additionally, Razak and Dosanjh [21] covered the significance of the condition monitoring system for identifying VIGV drift.

Compressor fouling has an impact on the performance of gas turbines. When sticky particles accumulate on the compressor's annulus passage, including the rotors and stators, compressor fouling occurs [22]. Ajoko and Tolumoye [23] studied monitoring industrial gas turbine performance, which can be affected by fouling, erosion, and other physical faults. The study's main goal is to predict an industrial gas turbine's performance using a data analysis process to check, balance, and monitor the behavior of the gas turbine while it is in operation. According to established facts, the drastic drop in performance was shown in the measurable performance parameters, which can be rectified and controlled with ambient temperature by regulating the intake supply fluid with dense air close to the intended specification. Finally, Ajoko and Tolumoye advised that, to avoid and minimize total gas turbine downtime, gas turbine operators must be familiar with such information for an early prognosis. Mishra [6] studied aero gas turbine compressor fouling and corrosion. The conclusion showed that the physical faults had been demonstrated to be well-addressed by compressor washing. The frequency of compressor wash must be carefully calculated from the perspectives of corrosion rate and performance degradation. The research [24,25] provides more information on fouling and erosion's impact on gas turbine performance. Adaptive performance models and simulations were conducted to estimate the fouling rate during operation to prevent a severe performance decline.

As discussed above, researchers have worked on the simulation of gas path faults and gas turbine performance degradation. However, only a few researchers have studied the performance degradation of all significant gas turbine components. Variable inlet guide vane drift and its combined effect with other physical faults remained unexplored. Therefore, this study aims to study the effect of variable inlet guide vane drift and its combined effect with fouling and erosion on the three-shaft gas turbine's performance at part-load operation. The effects on component isentropic efficiency and output parameters are studied and discussed. During the development of the engine performance model, secondary air or cooling systems and variable inlet guide vane scheduling were considered. With the help of engine manufacturer data, the gas turbine design point and off-design performance models have been built using GasTurb 13 and validated. Using the correlation between physical faults and performance parameters, fouling and erosion physical faults were introduced to the healthy engine model. Investigations of the combined effect of variable inlet guide vane drift with fouling and variable inlet guide vane drift with erosion on performance and output parameters are conducted. A three-shaft gas turbine engine was used as the study's case engine. It consists of six

primary gas-path components: a low-pressure compressor and turbine, a high-pressure compressor and turbine, a power turbine, and a combustion chamber. It has a single-shaft power turbine and a two-shaft gas generator. The gas generator includes the low and high-pressure compressor and turbine. The low-pressure and high-pressure turbines drive the low-pressure and high-pressure compressors. The power turbine has two stages and is a free axial turbine. The middle and last stages of the low- and high-pressure compressors are used to extract the cooling air. Figure 1 depicts a configuration for the three-shaft gas turbine.

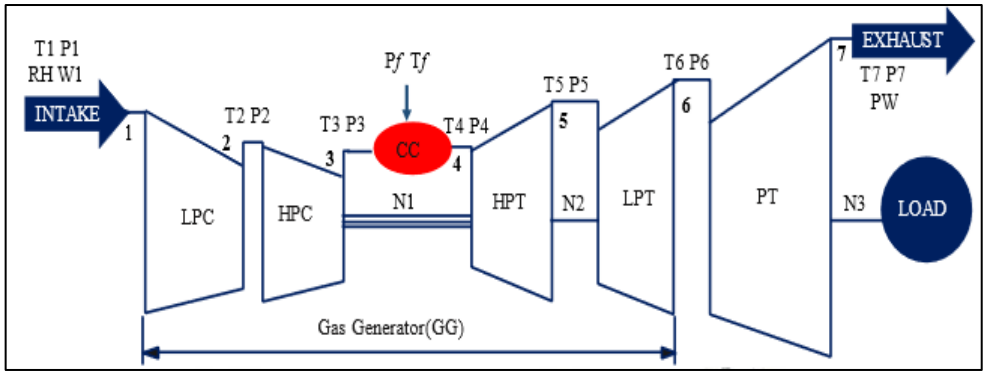

Figure 1: Configuration of a three-shaft gas turbine

2. Gas turbine performance model development

Many researchers used different methods to develop the gas turbine performance model. Using the method of determining Enthalpies and entropies at several key cycle points to assess the gas turbine's performance can be the most accurate method [26]. The performance model for gas turbines requires the development of design point and off-design models [27]. The design point model simulates the engine operating at the design load while computing all parameters at each component station. In off-design performance simulation, the design point is treated as one operating point. Combining the performance of each component of the gas turbine yields the overall performance of the actual gas turbine cycle [26,28]. The input data for developing the design point model was gathered from the technical manuals or catalogs of the manufacturer. For assessing the design point and off-design model, the energy balance approach and iteration and optimization methods were used to make the model accurate and verify the produced results [29]. If the model result matches the catalog data, then the model is considered an accurate model to predict engine performance [30].

2.1 Design Point Performance Modeling

The parameters at each station point of the engine were determined at design-point calculation. The ambient conditions, component efficiencies, compressor pressure ratio, inlet mass flow rate, air-fuel ratio in the combustion chamber, and turbine inlet temperature are among the input data. A design point performance model developed at the single operating point employing thermodynamic equations to calculate all unknown parameters. Examining the compatibility or energy equilibrium between components that use a common shaft is essential. MATLAB or another programming language can be used to create these thermodynamic equations. The model will continue to be improved until the percentage error becomes smaller and the energy is balanced. In this study, the performance model was developed using GasTurb 13 commercial software. The software employs the most accurate and promising method called determining enthalpy-entropy values at each gas path point. The input data for modeling the design and off-design performance and model validation are gathered from several sources. Most of the engine information, including thermal efficiency, power output, exhaust temperature, spool speeds, heat rate, inlet mass flow rate, pressure ratio, compressor, and turbine stages, was gathered from engine manufacturer datasheets. The remaining input parameters were gathered from scientific journal papers, and during model optimization, engineering judgments and estimated values were used.

The off-design model of the engine was assessed using the engine manufacturer data datasheet, which covered the entire operational spectrum. This included valuable information on thermal efficiency and power output in relation to ambient temperature. The ambient conditions adhered to ISO standards. The design point simulation involved calculating various thermodynamic parameters, such as pressure (P) and temperature (T) at different gas path points, fuel flow rate, compressor inlet air flow rate, component isentropic efficiencies, gas generator speed, net power output, and power turbine speed. While some of these parameters were readily available in the manufacturer's catalogue and technical documents, others needed to be calculated. The parameters needed to be determined low-pressure exit pressure and temperature, high-pressure compressor exit temperature, high-pressure turbine inlet pressure, high-pressure turbine exit pressure and temperature, low-pressure turbine exit pressure and temperature, power turbine exhaust pressure, each component isentropic efficiency and fuel flow rate. The input data shown in Table 1 were used to develop the engine performance model and to simulate all these parameters. Using the optimization constraints and parameters listed in Tables 2 and Table 3, the model has been optimized. Table 4 shows the objective function of the figure of merit.

Design point performance was developed using the known input parameters collected from the catalogue and available literature, along with some engineering judgments [9,31]. The secondary air system was considered; the percentage of the bleed air is depicted in Table 5.

Table 1: RB211-24G engine design point model input data (Data source: Engine catalogue and) [32]

Parameter	Unit	Value
Pressure ratio	-	20:1
Power output	mw	26.025
Thermal efficiency	%	35.8
Heat rate	kJ/kWh	10043
Exhaust mass flowrate	kg/s	92.2
Exhaust temperature.	°C	488
Turbine inlet temp.	°C	1193
HPC rotational speed	rpm	9445
LPC rotational speed	rpm	6643
FPT rotational speed	rpm	4950
HPC stages	-	6
LPC stages	-	7
LPT stages	-	1
HPT stages	-	1
FPT stages	-	2

Table 2: Parameters used as a constraint

Parameters	Unit	Minimum Value	Optimized values	Maximum Value
Heat rate	kJ/kWh	8852	10040.2	10043.5
Thermal efficiency	%	38	35.85	41
Exhaust Temperature (T5)	°C	460	479.076	496.7

Table 3: Parameters to be optimized

Variables	Unit	Min Value	Optimized Value	Max Value
HPT Rotor 1 Cooling air	%	3	5.1	5.4
HPT NGV 1 Cooling air	%	4	6.1	6.5
IPT Rotor 1 Cooling air	%	0.8	2.1	2.5
IPT NGV 1 Cooling air	%	0.8	2.1	2.5
Exhaust pressure ratio	-	1	1.1620	1.2
IPC Isentropic Efficiency	%	90	90	95
HPC Isentropic Efficiency	%	90	85	95
HPT Isentropic Efficiency	%	89	89.77	93
LPT Isentropic Efficiency	%	91	91.25	94
PT Isentropic Efficiency	%	89	89.63	92

Table 4: Objective function

Parameter	Unit	Value
Power output	kW	26025

Table 5: Secondary air fraction used during simulation

No	Components	Unit	Amount
1	Overboard air	%	0.5
2	HPT NGV 1 Cooling air	%	6.1
3	HPT Rotor 1 Cooling air	%	5.1
4	IPT NGV 1 Cooling air	%	2.1
5	IPT Rotor 1 Cooling air	%	2.1

The combustion chamber performance model was created using the energy balance equations presented in Equations 1, 2 and 3 [27], considering pressure loss.

$$\dot{m}_a h_3 + \dot{m}_f \times LHV \times \eta_{cc} = \left(\dot{m}_a + \dot{m}_f\right) h_4 \quad (1)$$

$$\dot{m}_f = \frac{\dot{m}_a (h_4 + h_3)}{\eta_{cc} \times LHV - h_4} \quad (2)$$

Compatibility of the components work:

$$W_{HPC} = W_{HPT},\ W_{LPC} = W_{LPT},\ W_{PT} = W_{\text{Load}} \quad (3)$$

where LHV is lower heating value, η_{cc} is combustion efficiency, $\dot{m}_a$ is inlet air mass flow rate, $\dot{m}_f$ is fuel mass flow rate, and h_3 is high-pressure compressor exit enthalpy. W_{LPC} is low pressure compressor work, W_{HPC} is high pressure compressor work, W_{lPT} is high pressure turbine work, W_{PT} is power turbine work, and W_{Load} is the load.

The model was optimized till the validation was matched. Finally, the output of the design point model was compared to the design parameters from the gas turbine product datasheet. As shown in Table 6, it was determined that the model has minimal discrepancies from the engine manufacturer data. Due to the agreement with the actual design values and very low variance, the design point values produced by the GasTurb-13 simulation were acceptable.

Table 6: The design point model output

Parameter	Units	Catalogue	GasTurb13 Model	% Error
Power Output	kW	26025	26025.5	0.0019
Thermal Efficiency	%	35.8	35.8	0
Pressure ratio	-	20:1	20:1	0
Fuel flowrate	kg/s	-	1.53281	-
Lower heating value	MJ/kg	-	47.16	-
Turbine Inlet temperature	°C	1193	1193	0
Exhaust Temperature	°C	488	479.5	1.74
Heat rate	kJ/(kW*h)	10043	10040.2	0.027

2.2 Off-design performance modelling

Following the successful development of the cycle design point calculations, an off-design model was developed. Off-design is the potential of the engine to run for the entire operating conditions, including the design point. It is all about state changes in ambient conditions and engine load. For instance, the ambient temperature may change drastically from winter to summer, which considerably impacts engine performance. As a result, the engine must perform efficiently at both design and off-design operating points. The initial step in off-design simulations is adapting the target engine's design point using the scaling approach and existing compressor and turbine mappings. The design point was scaled uniformly for each of the five component maps. Component matching is the second step in off-design, and it is done by employing the Newton-Raphson iterative process to ensure mass flow and work compatibility [27,33]. A suitable characteristics map comprising design point data was selected to alter the compressor and turbine maps. An additional coordinate was added to the component map digitization process, as suggested by Kurzke [34], to maintain accurate component matching. Component maps illustrate the interrelationship between corrected mass flow rate, corrected rotational speed, isentropic efficiency, and pressure ratio. The primary variables in the compressor and turbine maps were the intake mass flow rate (kg/s), rotational speed (rpm), inlet temperature (K), and inlet pressure to the compressor or turbine (kPa). To make using performance maps easier, corrected speed, corrected mass flow, pressure ratio, and isentropic efficiency were standardized using design point values. To scale the map, for example, for a high-pressure compressor, the values read from the map table must be corrected for Reynolds number effects, using the Reynolds Number Index (RNI), to ensure comparable to the design point efficiency and corrected flow. The auxiliary point beta for the map scaling point in GasTurb was set by default to be equal to 0.5 and the corrected speed to be equal to 1.0. The auxiliary point beta is required to be 0.5 to ensure that the engine is running at a point that is not close to the surging line. In addition, at the design point, the value of the corrected speed is also required to be 1, as it shows that the engine is running at full load. But at part-load operation, the corrected speed will be lower than 1. At first, the map will be scaled for the design point (subscript dp), and then the design point will be used as a reference point (subscript R, map), as explained in Equations (4) and (5) in the GasTurb 13 software manual [9].

$$\eta_{\text{dp,map}} = \eta_{R,map} \cdot f_{\eta,RNI} \tag{4}$$

$$\left(W\sqrt{\Theta_R}/\delta\right)_{dp,\,\text{map}} = \left(W\sqrt{\Theta_R}/\delta\right)_{R,\,\text{map}} \cdot f_{W,RNI} \tag{5}$$

Where $f\eta$, RNI is the Reynolds number index to correct the reference point efficiency read from the map, $\eta_{\text{dp, map}}$ is the scaled map design point efficiency, , $(W\sqrt{(\Theta R)}/\delta)_{\text{dp, map}}$ is the scaled map corrected mass flow, $\eta_{\text{R,map}}$ is the reference point efficiency from the unscaled map, $(W\sqrt{(\Theta R)}/\delta)_{\text{dp, map}}$ the reference point corrected mass flow from the unscaled map, The corrected temperature (Θ), and corrected pressure (δ) are expressed below in Equation 6 and 7, fW, RNI is the Reynolds number index to correct the reference point corrected mass flow read from the map.

$$\theta = \frac{T_o}{288.15K'} \tag{6}$$

$$\delta = \frac{P_o}{101.325\text{KPa}} \tag{7}$$

where P_0 and T_0 are the inlet pressure and temperature.

To be comparable with the design point efficiency dp, the value taken from the map must be corrected for Reynolds number effects using the terms fη,RNI and fW,RNI. Then, the map scaling factors will be calculated as follows: assuming RNI and fW,RNI, commonly assumed as fη,RNI = 0.99 and fη,RNI = 0.995 [9]. The Equations (8) to (11) that are used in GasTurb to scale component maps are explained in [9].

$$f_{\text{Mass}} = \frac{\left(\frac{W\sqrt{\Theta_R}}{\delta}\right)_{dp}}{\left(\frac{W\sqrt{\Theta_R}}{\delta}\right)_{R,\text{ map}} \cdot f_{W,RNI}} \tag{8}$$

$$f_{Eff} = \frac{\eta_{dp}}{\eta_{R,\text{ map}} \cdot f_{\eta,RNI}} \tag{9}$$

$$f_{P_3/P_2} = \frac{(P_3/P_2)_{dp}-1}{\left(\frac{P_3}{P_2}\right)_{R,\text{ map}}-1} \tag{10}$$

$$f_{\text{Speed}} = \frac{1}{N_{R,\text{ map}}} \tag{11}$$

Where $f_{p3/p2}$, f_{Mass}, f_{Speed} and f_{Eff} are pressure ratio, mass flowrate, speed scaling factors and efficiency, respectively. $N_{R,\text{ map}}$ is the compressor speed in the map. P_3 and P_2 are compressor exit and inlet pressures. Once all these scaling factors have been established, the efficiency, corrected mass flow, pressure ratio, and corrected speed were multiplied by the scaling factors to scale the map.

The suitable component maps were chosen at this point, and the cycle design point was matched with the selected map for accurate off-design simulations. To ensure that the flow and operation of the connected individual components are compatible, GasTurb 13 matches the component by the interaction of components. A steady-state off-design operating line is typically built using the Newton-Raphson iterative methodology because of its simplicity in non-linear systems [35]. After the relevant component maps were chosen, the off-design model was created and validated using manufacturer data, and the cycle design point was correlated. Commercial software, GasTurb 13, was used to develop the off-design model. Catalogue data validated the off-design model, including efficiency versus ambient temperature and power output versus ambient temperature. The VIGV scheduling and bleed air were taken into consideration in this study. The VIGV scheduling graph depicted in Figure 2 was imported into the engine simulation software. In this representation, the Y axis denotes the nominal angle of the variable inlet guide vane. In contrast, the X axis represents the non-dimensional spool speed of the low-pressure compressor (LPC). The non-dimensional spool speed is determined by dividing the LPC spool speed by the square root of the ambient temperature. The VIGV scheduling graph was gathered from the engine manufacturers' catalogue.

The off-design model generated data after incorporating the power output versus ambient temperature and VIGV scheduling into the software. The generated data was then compared with the validation data. The validation data and the model that produces the efficiency versus ambient temperature and power output versus ambient temperature were matched closely. At each operational point, the power output versus ambient temperature error from the validation data was 0.02%, while the 4.5% error was for the efficiency versus ambient temperature output data, as shown in Figures 3 and 4, respectively. Figures 3 and 4 showed that the off-design model results closely matched the validation data. This indicates the model is trustworthy and acceptable for predicting the gas turbine's performance. Another method of optimizing the off-design model was directly scheduling validation data into GasTurb 13, such as efficiency versus ambient temperature and power output versus ambient temperature. The graphs of power output and efficiency and the exhaust temperature in relation to ambient temperature are identical in both approaches. However, the second method's shortcoming is that it is impossible to simulate gas turbine performance when the engine operates at part-load. Due to the scheduled power output in the GasTurb 13 program, the limiting value option for power out will not be active. Suppose the physical faults are injected with manipulating flow capacity and isentropic efficiency at power output vs. ambient temperature scheduling. In that case, the output flow capacity and isentropic efficiency values will be reduced significantly more than the amount reduced to simulate the physical faults. This is because more heat must be delivered to maintain the power output unit, which lowers efficiency. For instance, Flow capacity and isentropic efficiency must be decreased by -7.5 and -2.5 percent, respectively, to simulate fouling at 100% fault severity. The gas generator must provide more heat when the fault factor is introduced to produce more high-temperature gas to compensate for the power loss caused by the deterioration of component characteristics and maintain the output power. The initial flow capacity and isentropic efficiency reduction will thus not be compared to the flow and isentropic efficiency in the normal condition but rather to the decreased value following the new power balance point. This means two factors contribute to the change in component performance: the first is a fault, such as a decrease in flow capacity of 7.5% and an isentropic efficiency of 2.5%, the second is the addition of more heat to maintain the power output production.

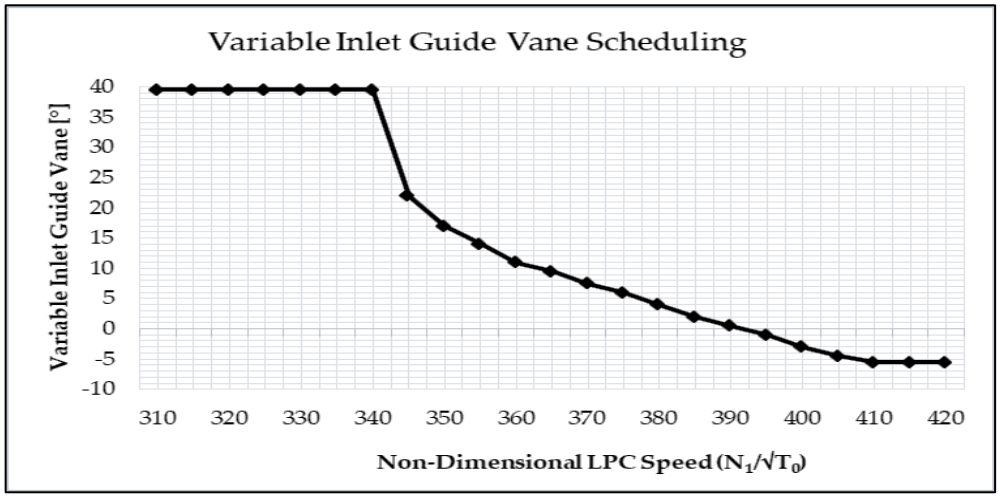

Figure 2: RB211-24G three-shaft gas turbine variable inlet guide vane schedule

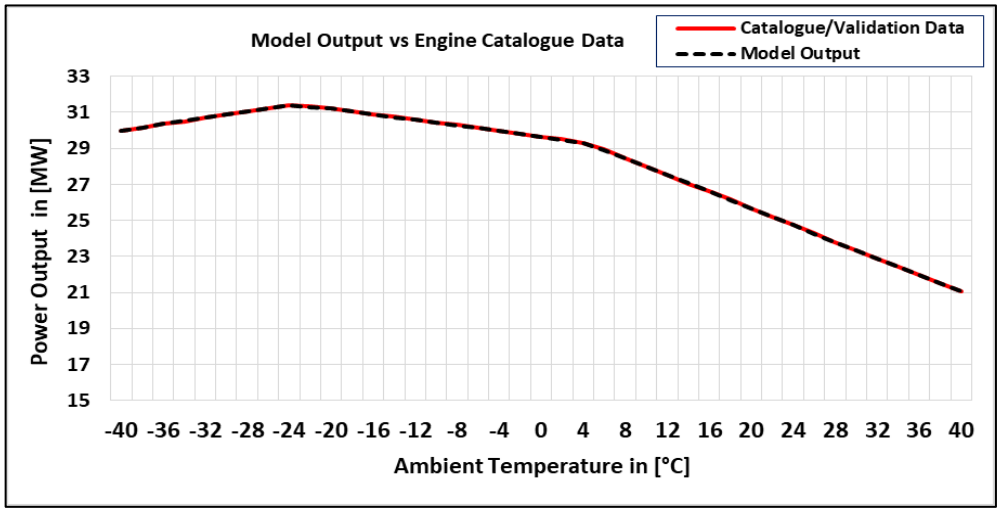

Figure 3: Validation of off-design model with power output

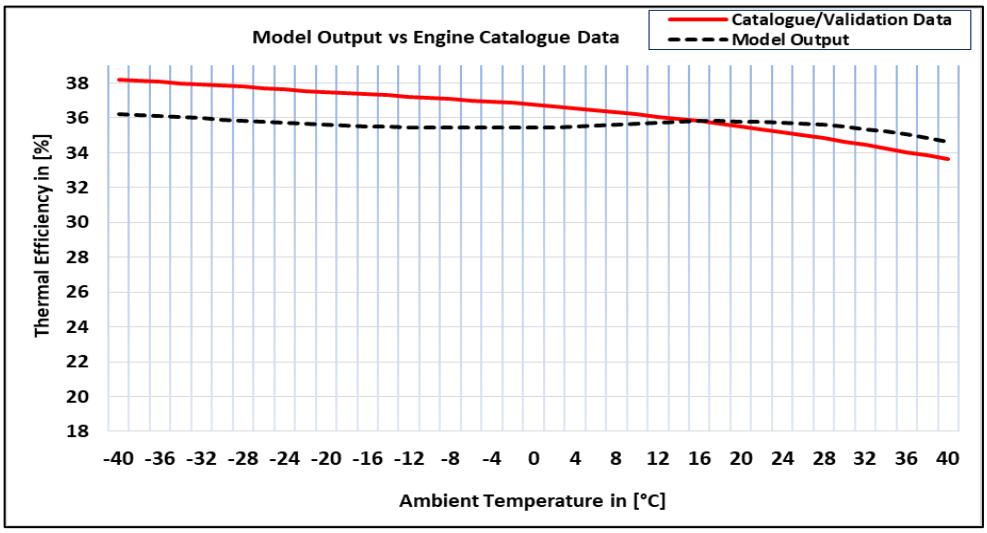

Figure 4: Validation of the Off-design model with Thermal efficiency

3. Physical fault simulation

Due to its vulnerability to different internal and external degradation factors, the performance of the gas-path components, in particular the compressor and turbine, is crucial to the engine's overall performance. There are two categories of causes for gas turbine deterioration. Mechanical failures include misalignment, imbalance, loose parts, bearing failures, and a lack of lubricating oil. The second reason for gas turbine deterioration is performance-related issues such as debris and fouling in

compressors, corrosion, edge erosion, improper combustion, increased clearance around blade tips, domestic object damage (DOD), and thermal distortion. Gas turbine performance deterioration can be temporary (recoverable by washing) or permanent (non-recoverable by washing). Permanent degradation requires replacement, whereas temporary degradation can be recovered during engine overhaul and operation. Fouling, erosion, corrosion, and blade tip clearance cause temporary deterioration, whereas airfoil distortion, untwist, and base distortions cause permanent deterioration. The most frequent cause of gas turbine performance decline is fouling and erosion. Hence, fouling and erosion physical faults combined with variable inlet guide vane drift were simulated in this study. Fouling is responsible for more than 70% of the overall loss of engine performance during the operation [36,37]. It is known that during gas turbine operation, a volume of air containing air pollutants enters the engine. Using health parameters, it is possible to monitor the decline in gas turbine engine performance [38]. Health parameters depict the performance changes caused by various defects. The ratio of degraded component isentropic efficiency and mass flow to those that are in good condition are called component health parameters, as shown in Equations (12) and (13) [39]. It defines that gas turbine performance degradation occurs when the health parameter is less than 1 but not when it is greater than 1 [38]. $H_{\Gamma,i}$, $H_{\eta,i}$ are health parameters.

$$H_{\Gamma,i} = \frac{\dot{m}_i\sqrt{T_i}}{P_i} / \left(\frac{\dot{m}_i\sqrt{T_i}}{P_i}\right)_{ref} \tag{12}$$

$$H_{\eta,i} = \eta_i/\eta_i \text{ ref} \tag{13}$$

where P_i is total pressure $H_{\Gamma,i}$, $H_{\eta,i}$ are health parameters, $\dot{m}_i$ is flow rate and η_i is isentropic efficiency.

Physical faults were introduced into the model to study how physical faults affect gas turbine performance. The relationship between physical faults and performance parameter deviations was used to simulate physical faults. The method used to simulate physical faults required a deliberate deviation in flow capacity and isentropic efficiency from the normal condition while maintaining the relationship between physical faults and performance parameters, as shown in Table 7. Prior to simulation and data generation from the model, the deviating values were scheduled in the software using the modifier option. As shown in Table 7, to simulate compressor fouling from 0% to 100% fouling severity level, the mass flow must be purposefully decreased at intervals of 0% to -7.5%, and isentropic efficiency must also be reduced at intervals of 0% to -2.5%. The flow capacity-isentropic efficiency relationship is 3:1 [39]. For instance, the flow capacity and efficiency will drop by -0.75 percent and -0.25 percent, respectively, at a 10 percent low- and high-pressure compressor fouling severity level scenario. This means 10% of -7.5% and -2.5%. For compressor erosion and turbine fouling simulations at 10% fault severity, the efficiency and mass flow reductions are -0.2% and -0.4%, respectively. However, it is important to note that erosion in the turbine increases flow capacity. Thus, to simulate turbine erosion at 10% fault severity, the isentropic efficiency was decreased by -0.2% while mass flow was increased by 0.4%.

Table 7: Health parameters and the physical fault relationships [37-39]

Physical fault	Flow capacity change (A)	Isentropic efficiency change (B)	Ratio A:B	Range
Compressor fouling	$\Gamma_C\downarrow$	$\eta_C\downarrow$	3:1	(0,-7.5%) (0,-2.5%)
Compressor erosion	$\Gamma_C\downarrow$	$\eta_C\downarrow$	2:1	(0,-4%) (0,-2%)
Turbine fouling	$\Gamma_T\downarrow$	$\eta_T\downarrow$	2:1	(0,-4%) (0,-2%)
Turbine erosion	$\Gamma_T\downarrow$	$\eta_T\downarrow$	2:1	(0,+4%) (0,-2%)

4. Results and discussion

4.1 The combined effect of fouling with VIGV drift and erosion with VIGV drift on the component isentropic efficiency

After developing and validating the design point and off-design performance models, Fouling and erosion were simulated using the relationship between physical faults and health parameters shown in Table 7. The GasTurb 13's Modifier option was used to implant the physical faults using Isentropic efficiency and flow capacity. To simulate the engine model in deteriorated condition, the compressor maps and turbine maps must be updated using the following scaling factors [39] which are presented in Equation 14 -16.

$$SF_{\Gamma,C} = 1 + \frac{\Delta H_{\Gamma,C}}{100} \tag{14}$$

$$SF_{\eta,C} = 1 + \frac{\Delta H_{\eta,C}}{100} \tag{15}$$

$$SF_{\Gamma,T} = 1 + \frac{\Delta H_{\Gamma,T}}{100} \tag{16}$$

$$SF_{\eta,T} = 1 + \frac{\Delta H_{\eta,T}}{100} \quad (17)$$

where $SF_{\eta,C}$ and $SF_{\Gamma,C}$ are the scaling factors of the compressor efficiency and flow capacity, $SF_{\Gamma,T}$ and $SF_{\eta,T}$ describe the scaling factors of the turbine and compressor flow capacity and efficiency . In contrast, $\Delta H_{\Gamma,C}$ and $\Delta H_{\eta,C}$ are the change of compressor flow capacity and efficiency, $\Delta H_{\Gamma,T}$ and $\Delta H_{\eta,T}$ are the change of turbine flow capacity and efficiency.

After implanting physical faults using the relations, the combined effect of fouling and variable inlet guide vane drift and erosion and variable inlet guide vane drift on component isentropic efficiency were investigated. Five different drift angles at 100% fouling and erosion fault severity levels were simulated. The VIGV drift angles were -6.5°, -3.5°, 0°, 3.5°, and 6.5°. The part load ranges were from 100% to 60% incremented by 10%. The combined effect of fouling and VIGV drift and the combined effect of erosion and VIGV drift on the main components of isentropic efficiency are shown in Figures 5 (a) to (j).

Figures 5(a) to 5(j) show the combined effect of variable inlet guide vane and fouling and the combined effect of variable inlet guide vane and erosion on the component isentropic efficiency at part-load operation: 100%, 90% Load, 80% Load, 70% load, and 60% Load. The fouling and erosion severity was 100%, and the VIGV drift angles were -6.5°, -3.5°, 0°, 3.5°, and 6.5°.

Figure 5(a) shows LPC's isentropic efficiency deviation when LPC fouling and VIGV drift occur simultaneously. The results show that the highest deviation of LPC isentropic efficiency was recorded when VIGV drift was at -6.5° and 100% fouling severity existed simultaneously. In contrast, thelowest deviation was shown when VIGV drift was at 6.5° and 100% fouling severity existed simultaneously. The result also shows that the deviation of lower drift is greater than the deviation of up VIGV drift for each load. Figure 5(b) shows thedeviation of HPC's isentropic efficiency when HPC fouling and VIGV drift occur at the same time. and 6.5°, respectively. Figure 5(c) shows the deviation of HPT's isentropic efficiency when HPT fouling and VIGV drift occur at the sametime. The isentropic efficiency is between -2.8% and -2.88%. This shows that the variation of VIGV drift on HPT isentropic efficiency has little effect on increasing the deviation. It is for two reasons:

1. The variable inlet guide vane, which regulates the mass flow rate, is mounted in the low-pressure compressor, and the low-pressure compressor shares the same shaft with the low-pressure turbine.
2. Downstream components (turbines) are less exposed to fouling than upstream components (compressors).

The results show that,although the deviation magnitude is different, the trend is similar to that of LPC's isentropic deviation. The highest and lowest deviations occurred at VIGV angle of -6.5° Figure 5(d) shows the deviation of LPT's isentropic efficiency when LPT fouling and VIGV drift occur at the same time. The results show that the highest deviation of LPT isentropic efficiency was recorded when VIGV drift was at 6.5° and 100% fouling severity existed at the same time. In contrast, the lowest deviation was shown when VIGV drift was at -6.5° and 100% fouling severity existed at the same time. The result also indicates that the deviation of lower drift is less than that of up VIGV drift for each load. Figure 5(e) shows the deviation of PT's isentropic efficiency when PT fouling and VIGV drift occur at the same time. The results show that the deviation is minimal. At 100% load and 90% Load, the deviationof PT isentropic efficiency increases at each VIGV drift angle. Figures 5(f) and 5(g) show the deviation of LPC and HPC isentropic efficiency when LPC erosion and VIGV drift occur concurrently and when HPC erosion and VIGV drift occur concurrently, respectively. The results show that in both LPC and HPC components, the highest deviation of isentropic efficiency was recorded at a down VIGV drift of -6.5°, while the lowest deviation was shown when the VIGV drift was at 6.5 at each load. Figure 5(h) shows the deviation of HPT isentropic efficiency when HPT erosion and VIGV drift occur concurrently, and the result shows the same trend as the trend shown in the LPC and HPC isentropic deviation due to the combined effect of erosion and VIGV drift. Figure 5(i) shows the deviation of LPT's isentropic efficiency when LPT erosion and VIGV drift occur at the same time. The results show thatthe highest deviation of LPT isentropic efficiency was recorded when VIGV drift was at 6.5° and 100% erosion severityexisted at the same time. In contrast, the lowest deviation was shown when VIGV drift was at -6.5° and 100% erosion severity existed at the same time. The result also shows that the deviation of the lower drift is less than that of the up VIGVdrift for each load. Figure 5(j) shows the deviation of PTisentropic efficiency when HPT erosion and VIGV drift occur concurrently, and the result shows the same trend as the trendshown in the LPC, HPC, and HPT isentropic deviation due tothe combined effect of erosion and VIGV drift. But the deviation magnitude is different and minimal in PT.

After simulating the combined effect of variable inlet guide vane and fouling and the combined effect of variable inlet guide vane and erosion on the component isentropic efficiency at part-load operation, the combined effect of variable inlet guide vane and fouling and the combined effect of variable inlet guide vane and erosion on gas turbine output parameters such as low-pressure compressors exit temperature, low-pressure compressor exit Pressure, high-pressure compressor exit pressure, high-pressure turbine exit pressure, high -pressure compressor exit temperature, low-pressure turbine exit pressure, fuel flow, power turbine exit temperature, low-pressure speed, high-pressure speed at part-load operation, 100%, 90% Load, 80% Load, 70%, Load, 60% Load has been simulated. The fouling and erosion severity was 100%, and the VIGV drift angles were, -6.5°, -3.5°, 0°, 3.5°, and 6.5°. The results are shown in Figures 6(a) to (j).

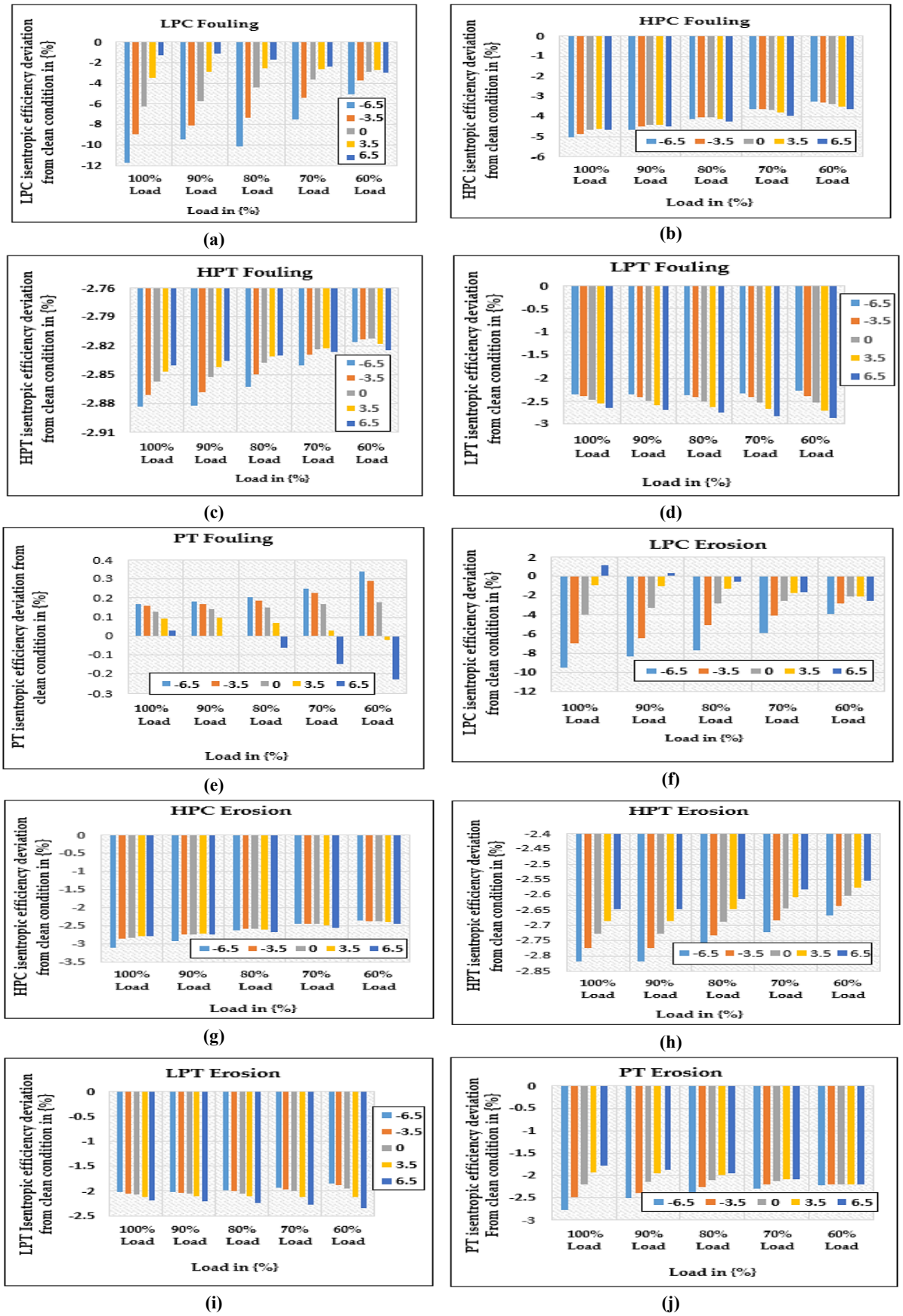

Figure 5: Deviation of component isentropic efficiency: (a) LPC fouling with VIGV drift, (b) HPC fouling with VIGV drift, (c) HPT fouling with VIGV drift, (d) LPT fouling with VIGV drift, (e) PT fouling with VIGV drift, (f) LPC erosion with VIGV drift, (g) HPC erosion with VIGV drift, (h) HPT erosion with VIGV drift, (i) LPT erosion with VIGV drift, (j) PT erosion with VIGV drift

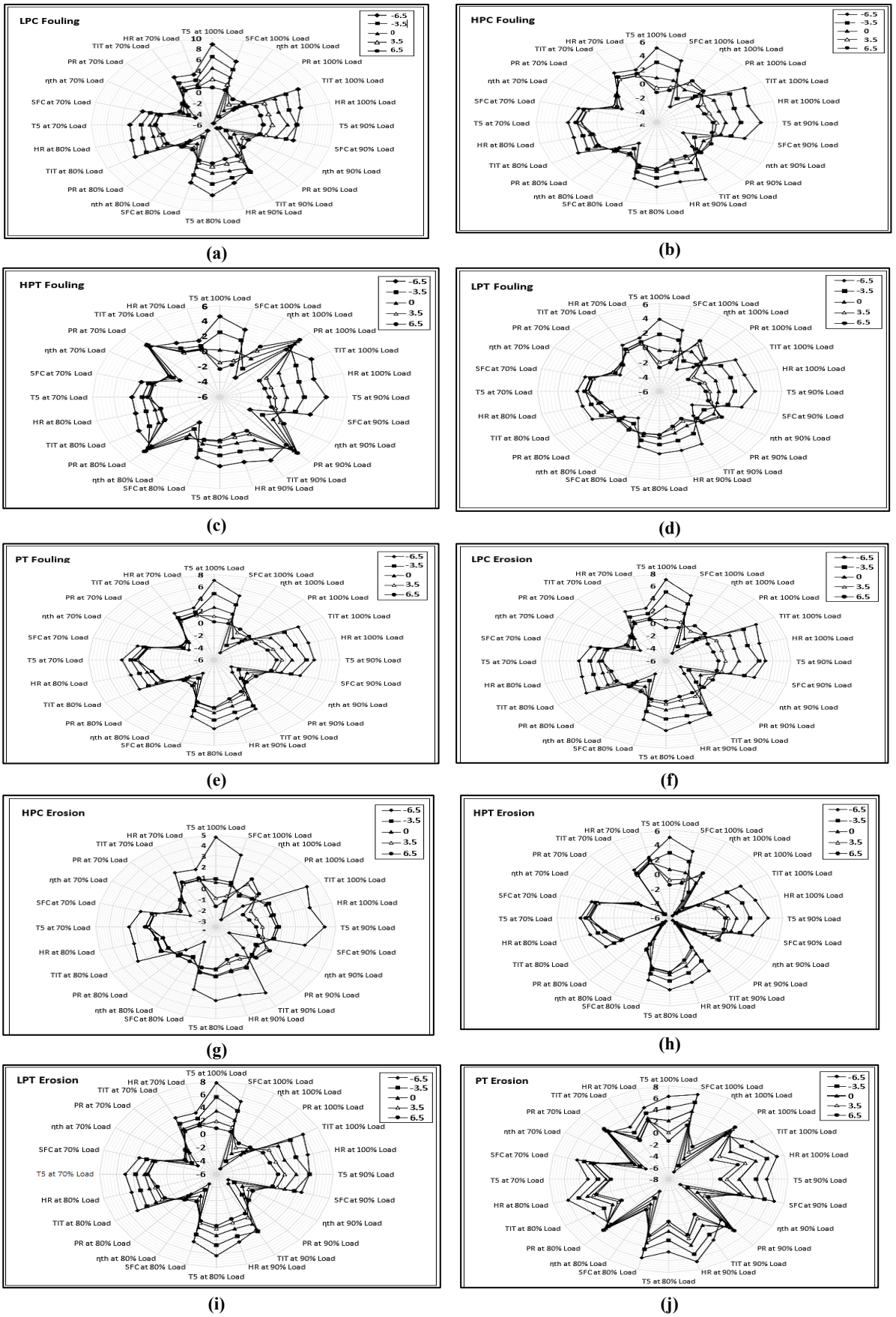

Figure 6: Deviation of Gas turbine output parameters: (a) LPC fouling with VIGV drift, (b) HPC fouling with VIGV drift, (c) HPT fouling with VIGV drift, (d) LPT fouling with VIGV drift, (e) PT fouling with VIGV drift,(f) LP Cerosion with VIGV drift, (g) HPC erosion with VIGV drift, (h) HPT erosion with VIGV drift, (i) LPT erosion with VIGV drift, (j) PT erosion withVIGV drift

Figures 6 (a-j) show how output parameters change at different loads (100% Load, 90% Load, 80% load, and 70% load) when fouling and VIGV drift are concurrently present. The fouling and erosion severity were applied at 100%, and the VIGV drift angles, -6.5°, -3.5°, 0°, 3.5°, and 6.5° were considered. The fouling and erosion severity were applied at 100%. Figure 6 (a) shows the deviation of output parameters when LPC fouling and VIGV drift occur at the same time. The results show that the deviations of T5, SFC, TIT, and HR were increasing while the deviations of ɳth and PR decreased at each load and VIGV drift. The highest deviation of the output parameters was observed when VIGV drift was at -6.5° and 100% fouling severity existed at the same time. In comparison, the lowest deviation was shown when VIGV drift was at 6.5, and 100% fouling severity existed at the same time for all parameters at each load and VIGV drift. Figure 6 (b) shows the deviation of output parameters when HPC fouling and VIGV drift occur at the same time. The results show the same trend as the output parameter deviation shown in the LPC due to the combined effect of fouling and VIGV drift. But the magnitude of the output parameter deviation was lower than the deviation shown due to LPC faults. Figure 6 (c) shows the deviation of output parameters when HPT fouling and VIGV drift occur at the same time. The results show that, except for the up VIGV drift angle of 6.5°, the deviations of T5, SFC, PR, TIT, and HR were increasing while the deviation of ɳth was decreasing at each load and VIGV drift. This occurred for two reasons:

1) A gas turbine is a complex, nonlinear system. It works through the interaction of all the components, which means the work and energy between the components that share the same shaft must be matched. But because of its nonlinearity, some discrepancy is expected to occur.
2) It is because the GasTurb software works on a dynamic basis. That means when fault factors are injected into component characteristics, the gas generator needs to produce more high-temperature gas to compensate for the power loss caused by the decline of component characteristics because the unit's output power should be kept unchanged [36].

Thus, increasing temperature causes exhaust temperature, specific fuel consumption, turbine inlet temperature, and heat rate to increase while thermal efficiency decreases. Figure 6 (d) depicts the output parameter deviation when LPT fouling and VIGV drift occur concurrently. Figure 6 (e) depicts the output parameter deviation when concurrent PT fouling and VIGV drift occur. The LPT and PT fouling graphs show the same trend as the output parameter deviation shown in the LPC and HPC due to the combined effect of fouling and VIGV drift. But the magnitude of exhaust temperature deviation is increased due to PT faults, while it is minimal due to LPT faults. This is because The VIGV mounted to the low-pressure compressor adjusts the mass flow rate. And it is worth mentioning that the low-pressure compressor and low-pressure turbine share the same shaft. Figure 6 (f) shows the deviation of output parameters when LPC erosion and VIGV drift occur at the same time. The results show that, except for the VIGV drift of 6.5°, the deviation of T5, SFC, TIT, and HR was increasing while the deviation of ɳth and PR decreased at each load and VIGV drift. It is also observed that the highest deviation of the output parameters occurred when VIGV drift was at -6.5, and 100% erosion severity existed at the same time. In comparison, the lowest deviation was shown when VIGV drift was at 6.5, and 100% erosion severity existed at the same time for all parameters at each load and VIGV drift. Figure 6 (g) shows the deviation of output parameters when HPC erosion and VIGV drift occur at the same time. The results show the same trend as the output parameter deviation in the LPC due to the combined effect of erosion and VIGV drift. But the magnitude of the output parameter deviation was lower than the deviation shown due to LPC faults. Figure 6 (h) shows the deviation of output parameters when HPT erosion and VIGV drift occur at the same time. The results show that the ɳth and PR deviations were decreasing at VIGV drift angles of -6.5°, -3.5°, and 0°, where they increased at 3.5° and 6.5° VIGV drifts. The deviations of T5, SFC, and TIT HR were increasing at VIGV drift angles of -6.5°, -3.5°, and 0°, where they decreased at 3.5° and 6.5° VIGV drifts. Figure 6 (i) depicts the output parameter deviation when LPT erosion and VIGV drift occur concurrently, and the result follows the same trend as the output parameter deviation shown when HPC erosion and VIGV drift are combined and exist. But the output parameter deviation due to LPT erosion and VIGV drift is greater than the output parameter deviation due to the combined effect of HPC erosion and VIGV drift at each load. Figure 6 (j) depicts the output parameter deviation when PT erosion and VIGV drift occur concurrently. The result shows that the deviation of ɳth is decreasing at each load and VIGV drift angle while the deviation of other parameters is increasing, except T5 and TIT at a VIGV drift angle of 6.5°.

5. Conclusion

The results showed that the upstream components are more affected by fouling, while the downstream components are affected by erosion. It is also seen that VIGV drift has a significant impact on the gas turbine's performance. When component fouling and VIGV drift are combined and exist, and when component erosion and VIGV drift are combined, the highest isentropic efficiency deviation is shown in the LPC. In contrast, the lowest deviation is shown in the LPT. The combined effect of fouling and up-VIGV drift and the combined effect of erosion and up-VIGV drift show a small deviation due to offsetting the isentropic efficiency decline caused by fouling and the isentropic efficiency decline caused by erosion. Furthermore, the combination of fouling and down-VIGV drift and erosion and down-VIGV drift reduced the component's isentropic efficiency. It was observed that the deviation of component isentropic efficiency and output parameters increases as the load increases. The combined effect of fouling and down-VIGV drift and the combined effect of erosion and down-VIGV drift caused the exhaust temperature to have the highest deviation at each load and VIGV drift angle. In general, in this paper, the deviation of isentropic efficiency and output parameters due to the combined effects of fouling and VIGV drift and the combined effects of erosion and VIGV drift at part-load operation are studied and discussed. The results will be very helpful in developing a fault detection, isolation, and identification model. The authors suggest that future research could use the results presented in this paper to develop a diagnosis model using machine learning.

Nomenclature

HPC	High-pressure compressor
LPC	Low-pressure compressor
LPT	Low-pressure turbine
HPT	High-pressure turbine
PT	Power turbine
T24	Low-pressure compressor exit Temperature
P24	Low-pressure compressor exit Pressure
P3	High-pressure compressor exit pressure
P43	High-pressure turbine exit pressure
T3	High -pressure compressor exit Temperature
P47	Low-pressure turbine exit pressure
FF	Fuel flow
T5	Power turbine exit temperature
N1	Low-pressure speed
GT	Gas Turbine
N2	High-pressure speed
CC	Combustion chamber
VIGV	Variable inlet guide vane
NGV	Nozzle guide vane
VAN	Variable area nozzle
VSV	Variable stator vane
VBV	Variable bleed valve
RVDT	Rotary variable displacement transducer
RNI	Reynolds number index
DOD	Domestic object damage
dp	Design point

Acknowledgements

For providing the resources, the authors are thankful to Universiti Teknologi PETRONAS.

Author contributions

Conceptualization, W. Salilew, Z. Abdul Karim and T. Lemma; software, Z. Abdul Karim and T. Lemma; data curation, W. Salilew; writing—original draft preparation, Z. Abdul Karim and T. Lemma. All authors have read and agreed to the published version of the manuscript.

Funding

Universiti Teknologi PETRONAS provided funding for this study under grant number YUTP-FRG, Cost Center 015LC0-347.

Data availability statement

Not applicable.

Conflicts of interest

The authors of the current work do not have a conflict of interest.

References

[1] Z. Li, S. S. Zhong, and L. Lin, Novel gas turbine fault diagnosis method based on performance deviation model, J. Propuls. Power, 33 (2017) 730–739. https://doi.org/ 10.2514/1.B36267

[2] O. Towoju, Impact of Cooling Fluid Temperature on the Structural Integrity of Gas Turbine Stator Blades, Eng. Technol. J., 41 (2023)1-9. http://doi.org/10.30684/etj.2023.138881.1409

[3] A. J. Abdulah, M. Z. Khalifa, and A. J. O. Hanfesh, Reducing vibrations generated in a gas turbine model MS9001E used in south Baghdad power plant station by improving the design of bearings with damper , Eng. Technol. J., 39 (2021) 1454-1462. http://doi.org/10.30684/etj.v39i9.2134

[4] G. Merrington, O. K. Kwon, G. Goodwin, and B. Carlsson, Fault detection and diagnosis in gas turbines, Proc. ASME Turbo. Expo., 5 (1990)1-10.https://doi.org/10.1115/90-GT-339

[5] H.I.H Saravanamuttoo and A.N Lakshminarasimha, A preliminary assessment of compressor fouling, American Society of Mechanical Engineer, 1985.

[6] R. K. Mishra, Fouling and Corrosion in an Aero Gas Turbine Compressor, J. Fail. Anal. Prev., 15 (2015) 837–845. https://doi.org/10.1007/s11668-015-0023-8

[7] Ihor. S. Diakunchak, Performance deterioration in industrial gas turbines, Proc. ASME Turbo. Expo., 4 (1991)1-8.https://doi.org/10.1115/91-gt-228

[8] Singh Grewal, M. Gas turbine engine performance deterioration modelling and analysis supervisor, cranfield institute of technologyschool of mechanical engineering ph.d thesis,1988.

[9] G. Gmbh, GasTurb 13 Design and Off-Design Performance of Gas Turbines, 85221 Dachau, Max Feldbauer Weg 5, Germany, 2018. http://www.gasturb.de

[10] North Atlantic Treaty Organisation, Performance Prediction and Simulation of Gas Turbine Engine Operation for Aircraft , Marine , Vehicular , and Power Generation, Estimation et simulation des performances du fonctionnement, 2007.

[11] M. Tahan, E. Tsoutsanis, M. Muhammad, and Z. A. Abdul Karim, Performance-based health monitoring, diagnostics and prognostics for condition-based maintenance of gas turbines: A review, Appl. Energy, 198 (2017) 122–144. https://doi.org/10.1016/j.apenergy.2017.04.048

[12] F. Haglind, Variable geometry gas turbines for improving the part-load performance of marine combined cycles - Gas turbine performance, Energy, 35 (2010) 562–570.https://doi.org/10.1016/j.energy.2009.10.026

[13] J. H. Kim, T. W. Song, T. S. Kim, and S. T. Ro, Dynamic simulation of full start-up procedure of heavy-duty gas turbines, J. Eng. Gas Turbines Power, 124 (2002) 510–516. https://doi.org/10.1115/1.1473150

[14] Bringhenti, C, Tomita, JT, de Sousa Ju´nior, F, and Barbosa, JR. 2006.Gas Turbine Performance Simulation Using an Optimized Axial Flow Compressor, Proceedings of the ASME Turbo Expo 2006: Power for Land, Sea, and Air. Turbomachinery, Parts A and B. Barcelona, Spain. Vol. 6, pp. 1941-1948. ASME. https://doi.org/10.1115/GT2006-91225

[15] W. M. Salilew, Z. A. A. Abdul Karim, T. A. Lemma, A. D. Fentaye, and K. G. Kyprianidis, Predicting the Performance Deterioration of a Three-Shaft Industrial Gas Turbine, Entropy, 24 (2022) 1052.https://doi.org/10.3390/e24081052

[16] T. W. Song, T. S. Kim, J. H. Kim, and S. T. Ro,Performance prediction of axial flow compressors using stage characteristics and simultaneous calculation of interstage parameters, Proc. Inst. Mech. Eng. A: J. Power Energy, 215 (2001) 89-98. https://doi.org/10.1243/0957650011536598

[17] A. Salar, S. M. Hosseini, B. R. Zangmolk and A. K. Sedigh, Improving Model-Based Gas Turbine Fault Diagnosis Using Multi-Operating Point Method, 2010 Fourth UKSim European Symposium on Computer Modeling and Simulation, Pisa, Italy, 2010, 240-247. https://doi.org/10.1109/EMS.2010.47

[18] A. Tsalavoutas, K. Mathioudakis, A. Stamatis, and M. Smith, Identifying faults in the variable geometry system of a gas turbine compressor, J. Turbomach., 123 (2001) 33-39.https://doi.org/10.1115/1.1330267

[19] Stamatis, A., Mathioudakis, K. and Papailiou, K. D. Adaptive simulation of Gas Turbine performance, Proceedings of the ASME Turbo Expo, 1989.

[20] S. Cruz-Manzo, S. Maleki, V. Panov, and Y. E. Zhang, Performance analysis of a twin-shaft gas turbine with fault in the variable stator guide vane system of the axial compressor, The Future of Gas Turbine Technology 9th International Gas Turbine Conference, Brussels, Belgium, 2018.

[21] A. M. Y Razak and M. S. Dosanjh, Application of an advanced performance monitoring system to detect an implanted fault on a twin spool aero derived gas turbine, Amsterdam, The Netherlands, 2002. https://doi.org/10.1115/GT2002-30022

[22] J. Enyia, I. Thank-God, D. Igbong, and J. Diwa, Industrial gas turbine on-line compressor washing for power generation, Int. J. Eng. Res. Technol., 4 (2015) 500-506.

[23] T.J .Ajoko, Performance monitoring of industrial gas turbine, Int. J. Eng. Sci. Invention, 3 (2014) 62–68.

[24] W. M. Salilew, Z. A. A. Abdul Karim, T. A. Lemma, A. D. Fentaye, and K. G. Kyprianidis, Three Shaft Industrial Gas Turbine Transient Performance Analysis, Sensors, 23 (2023) 1767.https://doi.org/10.3390/s23041767

[25] W. Molla Salilew, Z. Ambri Abdul Karim, and T. Alemu Lemma, Investigation of fault detection and isolation accuracy of different Machine learning techniques with different data processing methods for gas turbine, Alex. Eng. J., 61 (2022) 12635–12651.https://doi.org/10.1016/j.aej.2022.06.026

[26] Razak, A. M. Y. Industrial gas turbines: performance and operability, Woodhead Pub, 2007.

[27] M. B. Hashmi, T. A. Lemma, and Z. A. A. Karim, Investigation of the combined effect of variable inlet guide vane drift, fouling, and inlet air cooling on gas turbine performance, Entropy, 21 (2019) 1186. https://doi.org/10.3390/e21121186

[28] Razak, A. M. Y. 2013. Gas turbine performance modelling, analysis and optimization,Woodhead Publishing Limited, pp.423-514. https://doi.org/10.1533/9780857096067.3.423

[29] kurkz, Design-Point Calculations of Industrial Gas Turbines, ASME, 2020.

[30] S. I. Ao, L. Gelman, D. W. L. Hukins, A. Hunter, A. Korsunsky, and International Association of Engineers, Design and Off-Design Operation and Performance Analysis of a Gas Turbine, Proceedings of the World Congress on Engineering. London, 2, 2018

[31] J. H. Gao and Y. Y. Huang, Modeling and simulation of a aero turbojet engine with GasTurb, 2011 Int. Conf. Intell. Sci. Inf. Eng., 2011, 295-298. https://doi.org/10.1109/ISIE.2011.149

[32] M. S. Jasmani, Y. G. Li, and Z. Ariffin, Measurement selections for multicomponent gas path diagnostics using analytical approach and measurement subset concept, J. Eng. Gas Turbines Power, 133 (2011) 111701. https://doi.org/10.1115/1.4002348

[33] Y. Z. Chen, X. D. Zhao, H. C. Xiang, and E. Tsoutsanis, A sequential model-based approach for gas turbine performance diagnostics, Energy, 220 (2021) 119657. https://doi.org/10.1016/j.energy.2020.119657

[34] Kurzke, J. 2007.About Simplifications in Gas Turbine Performance Calculations. Proceedings of the ASME Turbo Expo 2007: Power for Land, Sea, and Air. Turbo Expo 2007. Montreal, Canada,Vol.3 1, pp. 493-501, ASME. https://doi.org/10.1115/GT2007-27620

[35] M. P. Boyce , C. B. Meher-Homji, and A. N. Lakshminarasimha Modeling and Analysis of Gas Turbine Performance Deterioration, J. Eng. Gas Turbines Power, 116 (1994) 46-52. https://doi.org/10.1115/1.2906808

[36] Efstratios Ntantis, Capability Expansion of Non-Linear Gas Path Analysis, PhD Thesis, Cranfield University, 2008.

[37] Y. Qingcai, S. Li, Y. Cao, and N. Zhao, Full and Part-Load Performance Deterioration Analysis of Industrial Three-Shaft Gas Turbine Based on Genetic Algorithm, Proceedings of ASME Turbo Expo 2016: Turbomachinery Technical Conference and Exposition, South Korea, 2016. https://doi.org/10.1115/GT2016-57120

[38] E. Mohammadi ,M. Montazeri-Gh, Simulation of full and part-load performance deterioration of industrial two-shaft gas Turbine, J. Eng. Gas Turbines Power, 136 (2014) 9. https://doi.org/10.1115/1.4027187

[39] W. M. Salilew, Z. A. A. Abdul Karim, T. A. Lemma, A. D. Fentaye, and K. G. Kyprianidis, The Effect of Physical Faults on a Three-Shaft Gas Turbine Performance at Full- and Part-Load Operation, Sensors, 22 (2022) 7150, https://doi.org/10.3390/s22197150